Journal of Hazardous Materials 170 (2009) 210–218

Contents lists available at ScienceDirect

Journal of Hazardous Materials

journal homepage: www.elsevier.com/locate/jhazmat

A theoretical approach to the deposition and clearance of fibers with variable size in the human respiratory tract

Robert Sturm*, Werner Hofmann

Department of Materials Engineering and Physics, University of Salzburg, Hellbrunner Strasse 34, 5020 Salzburg, Austria

ARTICLE INFO

Article history:
Received 16 December 2008
Received in revised form 27 April 2009
Accepted 28 April 2009
Available online 3 May 2009

Keywords:
Fiber
Monte Carlo model
Aerodynamic diameter
Lung clearance
Multicompartment model

ABSTRACT

In the study presented here, a mathematical approach for the deposition and clearance of rigid and chemically stable fibers in the human respiratory tract (HRT) is described in detail. For the simulation of fiber transport and deposition in lung airways an advanced concept of the aerodynamic diameter is applied to a stochastic lung model with individual particle trajectories computed according to a random walk algorithm. Interception of fibrous material at airway bifurcations is considered by implementation of correction factors obtained from previously published numerical approaches to fiber deposition in short bronchial sequences. Fiber clearance is simulated on the basis of a multicompartment model, within which separate clearance scenarios are assumed for the alveolar, bronchiolar, and bronchial lung region and evacuation of fibrous material commonly takes place via the airway and extrathoracic path to the gastrointestinal tract (GIT) or via the transepithelial path to the lymph nodes and blood vessels.

Deposition of fibrous particles in the HRT is controlled by the fiber aspect ratio β in as much as particles with diameters <0.1 μm deposit less effectively with increasing β, while larger particles exhibit a positive correlation between their deposition efficiencies and β. A change from sitting to light-work breathing conditions causes only insignificant modifications of total fiber deposition in the HRT, whereas alveolar and, above all, tubular deposition of fibrous particles with a diameter ≥0.1 μm are affected remarkably. For these particles enhancement of the inhalative flow rate results in an increase of the extrathoracic and bronchial deposition fractions. Concerning the clearance of fibers from the HRT, 24-h retention is noticeably influenced by β and, not less important, by the preferential deposition sites of the simulated particles. The significance of β with respect to particle size may be regarded as similar to that determined for the deposition scenarios, while breathing conditions do not have a valuable effect on clearance.

1. Introduction

1.1. General aspects

In the past decades deposition of aerosol particles in the human respiratory tract (HRT) has attracted considerable scientific attention due to its significance in occupational health. Numerous studies on the behaviour of spherical particles in bronchial airways could find an unequivocal evidence for the dependence of health effects on the site of preferential particle deposition as well as the physical properties of the inhaled particulate matter [1–3]. A highly important role concerning the particle-induced generation of lung diseases has been attributed to fibers which per definition are elongated particles with approximately cylindrical shape, a length exceeding 5 μm, and an aspect ratio (i.e. the ratio of the length to the diameter) greater than 3 [4,5]. As exhibited by a limited number of experiments dealing with the deposition of fibrous material in bronchial airway casts [6–8], principal factors affecting the deposition patterns and efficiencies of fibers include the aerodynamic properties of these particles, expressed by the aerodynamic diameter, and the nature of convective flow in single airway bifurcations. Studies already carried out in the 1970s have underlined the important fact that the aerodynamic diameter of a fiber chiefly depends on its cylindrical diameter but is only slightly influenced by its length [9]. Contrary to spheres there are four main mechanisms controlling the deposition of fibers in the HRT, namely inertial impaction, interception, sedimentation, and diffusion (Fig. 1). By some authors also a mechanism called electrostatic precipitation is associated with fiber deposition [10], but due to the non-availability of experimental data the role of this deposition force is not quite clear hitherto. Inertial impaction and interception mainly occur in the larger bronchial airways, where flow velocities are enhanced and fibers are propelled out of bending flow streamlines due to their momentum. While impaction commonly increases with the aerodynamic diameter, interception is dependent upon local Stokes

* Corresponding author. Tel.: +43 662 8044 5705; fax: +43 662 8044 150.
E-mail address: Robert.Sturm@sbg.ac.at (R. Sturm).

0304-3894/$ – see front matter © 2009 Elsevier B.V. All rights reserved.
doi:10.1016/j.jhazmat.2009.04.107

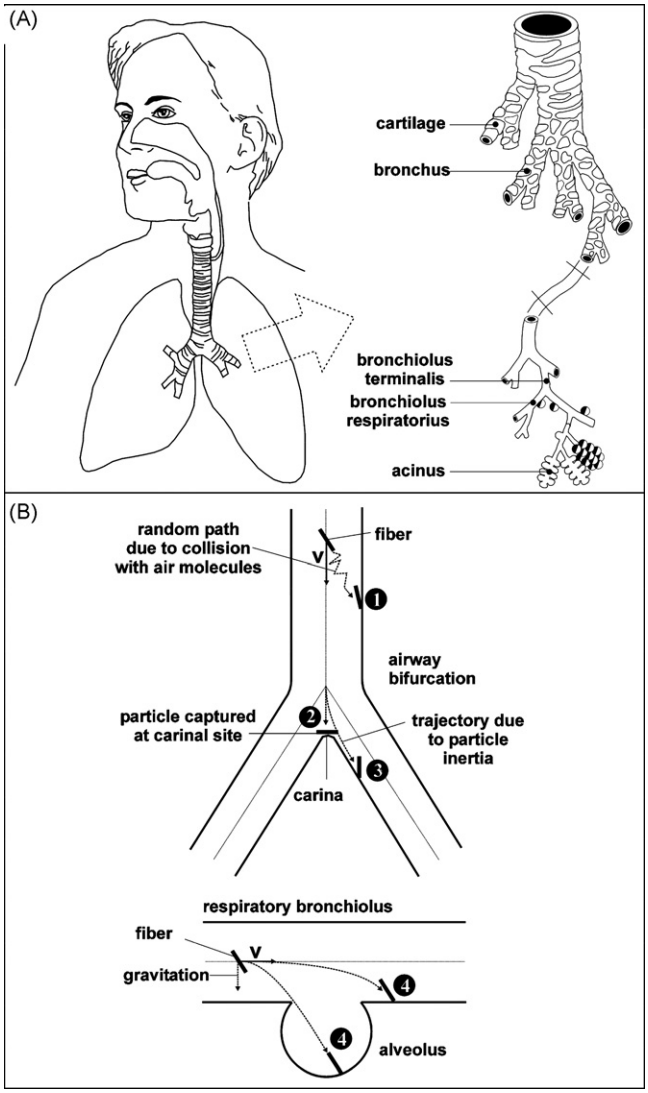

Fig. 1. (A) Architecture of the tracheobronchial tree and the pulmonary region responsible for the O_2–CO_2 gas exchange. (B) Mechanisms of fiber deposition in proximal and terminal (alveolated) airways of the HRT: (1) Brownian diffusion, (2) interception, (3) inertial impaction, (4) gravitational settling (sedimentation). Abbreviation: v – particle velocity vector.

number as well as fiber length, i.e. the longer a fiber, the higher its deposition by interception. Sedimentation, on the other side, is favoured by low flow velocity, therefore preferentially occurring in small airways. Diffusion describes the collisions between air molecules and airborne fibers and becomes highly important for particles smaller than 0.5 μm. Experiments, where rats were exposed to an atmosphere including variably sized glass fibers for several hours, indicated that fibers exceeding a length of 10 μm are mostly deposited in the extrathoracic region and penetrability of fibrous material into the rat lung drops sharply with aerodynamic diameter above 2 μm [11,12]. More current experiments using replica of the extrathoracic region and the proximal airways of the HRT mainly confirmed these previous findings in rats, but also considered the possibility of a penetration of long fibers into deeper regions of the lung in the case of low flow velocities and aerodynamic diameters around 1 μm [1,5,13].

The clearance of fibrous particles deposited in the HRT depends on both the site of deposition and the physical properties of the fibers. Fibrous material accumulated in the tracheobronchial airways is mainly transported on the surface of the mucus layer towards the larynx, where it is swallowed and passes into the gastrointestinal tract (GIT) [10]. Besides this mucociliary clearance taking place within the first 24 h after exposure to the fibrous aerosol, a part of the material deposited in the airway tubes is also subject to slow clearance mechanisms including the uptake of fibers by airway macrophages, epithelial transcytosis, as well as the temporary storage of the particles in the periciliary liquid layer and subsequent recapture by the mucus layer (Fig. 2) [14,15]. According to several inhalation experiments [16] the half-time of this slow bronchial clearance may vary between several days and weeks. Fibers deposited in small nonciliated airways and alveoli are affected by a strongly increased retention, and clearance from these distal deposition sites mainly takes place by translocation and disintegration [10]. Translocation represents the movement of an intact fiber either along the epithelial surface towards the terminal bronchioles or into and through the epithelium towards the interstitial tissue. The transport of the fibrous material is usually realized due to its ingestion by alveolar macrophages but smaller fibers may be also dislocated on the surfactant layer [10]. Disintegration, on the other hand, refers to the subdivision of a fiber into smaller segments and the dissolution of specific fiber components, whereby both phenomena are highly dependent upon the biodegradability of the material. Asbestos and man-made mineral fibers are practically not clearable by disintegration, whereas glass fibers exhibit a measurable clearance by this mechanism which negatively correlates with the length of the particles [17,18]. In general, alveolar clearance half-times of fibers smaller than 5 μm in length range from 100 to 150 days [10,16].

1.2. Modelling fiber deposition and clearance in the HRT – state of the art

Deposition models are highly appropriate for the detailed prediction of particle concentrations in specific regions of the HRT, where the experimental measurement is not feasible. Due to this advantage, mathematical approaches describing the behaviour of particles in the lung have become essential tools in medical science meanwhile. Concerning the deposition of fibers (expressed by spheres with respective aerodynamic diameters) in the HRT, preliminary theoretical models date back to the 1970s and subdivide the respiratory compartment into three distinct parts (head, tracheobronchial, and pulmonary region) [19,20]. Later approaches assume a single-path, dichotomous lung geometry, where inhaled particles are transported along an average airway trajectory [21–23]. These deposition models are limited to the prediction of regional fiber deposition in the HRT but are not able to generate reliable information regarding the distribution of particulate matter within a selected lung lobe or a single airway generation. This significant drawback was solved by the development of multiple-path deposition models considering a nonsymmetric, more realistic structure of the lung and thus allowing more site-specific predictions [24]. Currently, results of theoretical approaches to fiber deposition in single airway bifurcations were implemented in stochastic deposition models of the entire lung, thereby enabling the computation of rather precise generation-by-generation deposition plots [25]. Precise predictions of fiber deposition in the lungs are to a high extent based on respective numerical simulations investigating the behaviour of nonspherical particles in single airway bifurcations or small bifurcation sequences [6,7,37,38,41–43].

Mathematical models dealing with the clearance of inhaled particulate matter deposited in the HRT are so far limited to spherical insoluble particles, whereby various approaches to mucociliary clearance as well as slow bronchial and alveolar clearance mechanisms have been introduced [16,26–29]. Regarding the clearance of fibrous material, the human respiratory tract model (HRTM) introduced by the International Commission on Radiation Protection

(ICRP) partly considers differences of bronchial and alveolar clearance between spheres and fibers by the definition of respective clearance half-time correction factors [16]. Hitherto, these factors are independent of the deposition site and therefore represent a major simplification within the multicompartmental approach.

1.3. Main objectives of the study presented here

In this contribution two major objectives are pursued: First, the deposition of rigid and chemically stable fibers approximated by spheres with various aerodynamic diameters is modeled by using a Monte Carlo deposition algorithm based on a stochastic geometry of the human lung [25]. This model, which has been extensively validated with experimental data in the past two decades, allows the prediction of both regional and airway bifurcation-specific particle deposition patterns. Where experimental data of fiber deposition in human airway casts are available, they are compared with the model and discussed. Second, bronchial and alveolar clearance of the particles used for deposition modelling is crudely approximated by using an advanced multicompartment model which is based on the mathematical approach preliminarily introduced by Sturm and Hofmann [26]. The new model described here in detail has been extended by the alveolar compartment (see below), because this region of the lung seems to play a highly significant role in fiber clearance. Results of the clearance predictions are comprehensively discussed to get a preliminary impression of model reliability.

2. Description of the mathematical model

2.1. Fiber deposition

For the theoretical computation of fiber deposition in the HRT the widely used aerodynamic diameter concept is applied. By definition, the aerodynamic diameter, d_{ae}, refers to the diameter of a unit density sphere with identical aerodynamic characteristics as the particle of interest. Mathematically, this parameter is defined as [30]:

$$d_{ae} = d_{ev}\sqrt{\frac{1}{\chi}\times\frac{C_C(d_{ev})}{C_C(d_{ae})}\times\frac{\rho_p}{\rho_0}}, \tag{1}$$

with d_{ev}, χ, $C_C(d_{ev})$, $C_C(d_{ae})$, ρ_p, and ρ_0 denoting, respectively, the equivalent volume diameter, the dynamic shape factor, the Cunningham slip correction factor for particles with d_{ev}, the correction factor for particles with d_{ae}, the density of the particle ($g\,cm^{-3}$), and unit density ($1.0\,g\,cm^{-3}$). The equivalent volume diameter, d_{ev}, represents the diameter of a sphere with the same volume as the fibrous particle considered for deposition calculation. In the case of a fiber with perfect cylindrical shape, it is obtained from the formula:

$$d_{ev} = \sqrt[3]{1.5 d_p^3 \beta}, \tag{2}$$

where d_p represents the particle diameter and β the aspect ratio, i.e. the ratio between length and diameter of the fiber. The dynamic shape factor, χ, denotes a dimensionless constant that relates the drag force experienced by an irregularly shaped particle moving in air to the particle's equivalent volume diameter [30]. For a fibrous particle being transported with random orientation through the airway tubes of the tracheobronchial tree, χ can be written as [31]:

$$\frac{1}{\chi} = \frac{1}{3\chi_{//}} + \frac{2}{3\chi_{\perp}}. \tag{3}$$

In the equation noted above, $\chi_{//}$ is the dynamic shape factor of a given fiber oriented parallel to the direction of flow, whereas $\chi_{\perp}$ represents the dynamic shape factor of the fiber oriented perpendicular to the flow vector. The two factors are defined by the following equations [13]:

$$\chi_{//} = \frac{(4/3)(\beta^2-1)\beta^{-1/3}}{\left\{((2\beta^2-1)/\sqrt{\beta^2-1})\ln\left[\beta+\sqrt{\beta^2-1}\right]-\beta\right\}}, \tag{4}$$

$$\chi_{\perp} = \frac{(8/3)(\beta^2-1)\beta^{-1/3}}{\left\{((2\beta^2-3)/\sqrt{\beta^2-1})\ln\left[\beta+\sqrt{\beta^2-1}\right]+\beta\right\}}. \tag{5}$$

It has to be noted that in the current model fiber orientation in the more peripheral airways is assumed to be approximately parallel to the airway wall, thereby following recent findings obtained from experiments with glass fibers [39].

The Cunningham slip correction factor, C_C, considers the circumstance that small particles (<1 μm) settle faster than predicted by Stokes law because, contrary to the ideal assumptions of the law, the relative velocity of the gas right at the particle's surface significantly deviates from zero. Assuming the air conditions of the HRT, i.e. 100% relative humidity, 76 cm Hg atmospheric pressure, an air temperature of 37 °C, and a related mean free path of the air molecules of 0.0712 μm, C_C may be calculated according to the formula [16]:

$$C_C = 1 + \frac{1}{76d}\left[13.571 + 4.312\exp(-7.7672d)\right]. \tag{6}$$

In Eq. (6), d refers to a selected particle diameter (d_{ae} or d_{ev}). The slip correction factor presented here is a simplification, because Brownian rotation [40] affecting fiber diffusion to a certain degree is not considered in the current version of the model.

For particle deposition calculations the model provided by Koblinger and Hofmann [25] was used. This mathematical approach is based on a random walk algorithm, according to which each inhaled particle is transported along a randomly selected path through the tracheobronchial and acinar regions. By application of the so-called Monte Carlo simulation technique, large numbers of such particle trajectories (e.g. 10,000) may be generated to obtain statistically reliable data. A further improvement of the model with respect to more previous approximations is the use of a stochastic lung architecture providing a realistic variability of airway geometry and orientation within a specific lung generation. Morphometric data necessary for the generation of this probabilistic lung model were implemented into the approach, thereby using respective data sets of the tracheobronchial tree [32] and the acinar region [33]. For each morphometric parameter the distribution of the measured values was determined and related probability density functions were created [34], with the help of which the stochastic lung was constructed airway by airway.

Computation of particle deposition was carried out by the application of specific deposition formulae for Brownian diffusion, inertial impaction and sedimentation [24,25]. To account for interception representing an essential deposition force of fibers, correction factors for the bronchial airway generations 1–12 were computed which are based on numerical simulations of fiber behaviour within single airway bifurcations [35–38,41–43] and are expressed as functions of Stokes number, St, and aspect ratio, β. Hence, fiber deposition probability by interception, $dep_{f,i}$, in a bronchial airway, i, is derived from the deposition probabilities of related spheres, $dep_{s,i}$, as follows:

$$dep_{f,i} = dep_{s,i} C_i(St_i, \beta). \tag{7}$$

To further improve the statistics of the Monte Carlo simulations, for each particle entering the lung multiple deposition scenarios were computed by application of the statistical weight method [25]. Here, a unit weight, which was attributed to the particle after intruding into the trachea, was multiplied by $(1-p_i)$ at each bifurcation with p_i denoting the deposition probability at that bifurcation

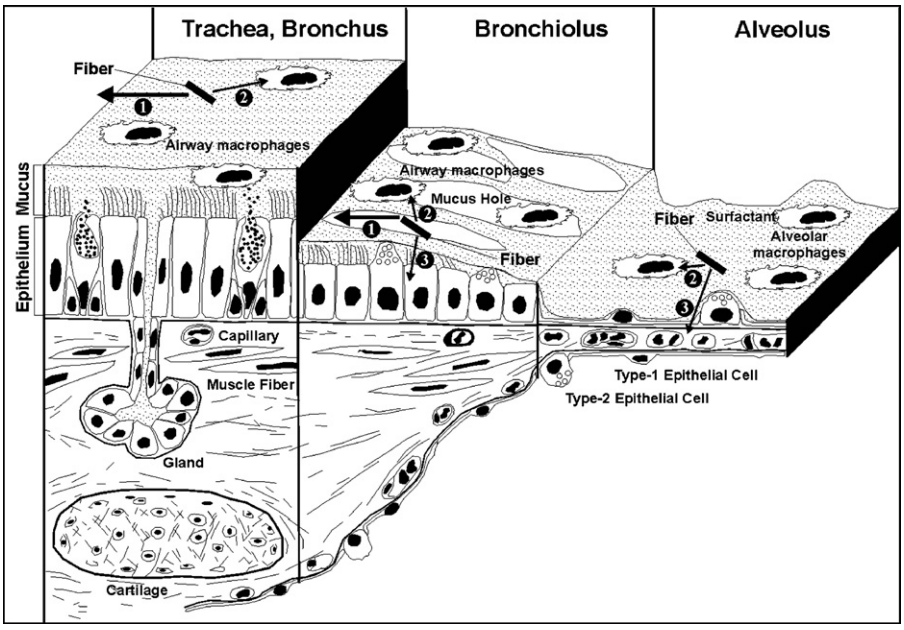

Fig. 2. Scheme exhibiting the basic histology of the bronchial, bronchiolar, and alveolar lung region and the main mechanisms of fiber clearance: (1) mucociliary clearance, (2) uptake by airway/alveolar macrophages, (3) transepithelial clearance [14,26–27].

unit. The final deposition fraction in a specific airway bifurcation was given by the product of the actual weight and the respective deposition probability.

Deposition scenarios were created by assuming standard breathing conditions suggested by the ICRP [16] (sitting breathing: tidal volume of 750 ml, breathing frequency of 12 min^{-1}; light-work breathing: tidal volume of 1250 ml, breathing frequency of 20 min^{-1}) and unit-density particles.

2.2. Clearance of fibrous particles

For the approximation of fibrous particle clearance from the HRT an expanded version of the multicompartment clearance model previously introduced by Sturm and Hofmann [26] was applied. Since the theoretical background of the mathematical approach was already described in detail in this preceding work, for the sake of brevity, only the most salient features of the model will be subject to an explanation in the contribution presented here. The multicompartment model with its single compartments and rate constants is schematically illustrated in Fig. 3. In general, three regions of the lung (i.e. alveolar, bronchiolar, and bronchial) characterized by differences concerning the clearance of deposited particulate matter are distinguished within the approach. Clearance in the bronchiolar and bronchial region is represented by four compartments, respectively, between which deposited mass is transferred with different velocity [16,26]. The gel layer compartment commonly refers to fast clearance, while the remaining compartments (sol layer, airway macrophage, and epithelium) refer to slow clearance mechanisms (particle uptake by airway macrophages, epithelial endocytosis and transcytosis, temporary storage of particles in the periciliary sol layer). In the alveolar region the gel and sol layer compartments have been replaced by a surfactant compartment. Transfer of particulate matter between the single lung regions takes place along a few paths, whereby macrophages and liquid layers lining the epithelial walls play an essential role in this context (Fig. 3). The gastrointestinal tract as well as the lymph and blood

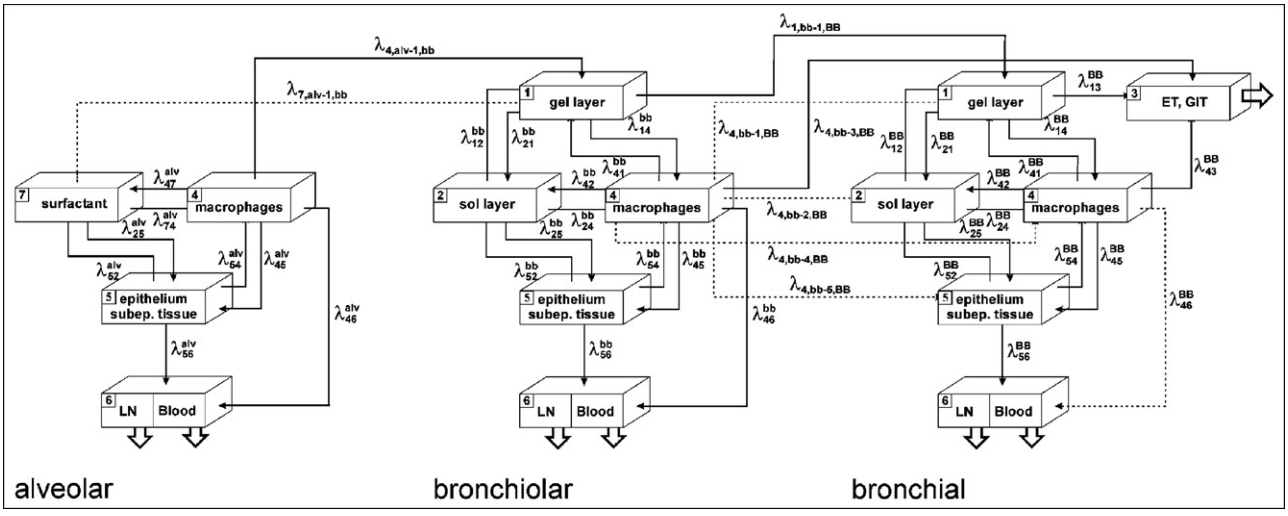

Fig. 3. Multicompartment model illustrating possible clearance paths in the bronchial, bronchiolar, and alveolar lung region (for detail see text). Dashed lines indicate those paths with strongly decreased probabilities.

vessels act as target compartments, to which the cleared particles are finally transported. In future models, the further fate of ultrafine particles in the lymph and blood vessels will be investigated more in detail to theoretically approximate the possible relationship between cardio-vascular insufficiencies and the exposure the ultrafine aerosols.

Mathematically, the temporary change of the particulate mass concentration in a given compartment, C_i, is described by the difference between the mass entering this compartment and the mass leaving the compartment:

$$\frac{dC_i}{dt} = \lambda_{ji}C_j + \ldots + \lambda_{ri}C_r - (\lambda_{ij} + \ldots + \lambda_{ir})C_i. \quad (8)$$

In Eq. (8) C_j–C_r denote those compartments of the model which are marked by a mass transfer to compartment C_i, λ_{ji}–λ_{ri} are the rate constants of incoming paths, and λ_{ij}–λ_{ir} represent the rate constants of the outgoing paths. Solution of the equation noted above yields:

$$C_i(t) = \left[C_i(t_0) - \frac{(\lambda_{ji}C_j + \ldots + \lambda_{ri}C_r)}{(\lambda_{ij} + \ldots + \lambda_{ir})}\right] \exp\left[-(\lambda_{ij} + \ldots + \lambda_{ir})t\right] + \frac{(\lambda_{ji}C_j + \ldots + \lambda_{ri}C_r)}{(\lambda_{ij} + \ldots + \lambda_{ir})} \quad (9)$$

As demonstrated in the previous study, rate constants hypothetically depend upon numerous particle characteristics and physiological parameters, from which particle size (and shape) seem to have an extraordinary importance [26]. In Eq. (9) $C_i(t_0)$ denotes the particulate mass concentration in compartment i at the time $t = 0$. By definition, initial particulate mass only occurs in the different liquid layer compartments (gel, sol, and surfactant), whereas in the remaining compartments the initial particle mass concentration is set to 0. The mass fraction of particles retained in the HRT after a certain time period, $R(t)$, is given by the simple formula

$$R(t) = 1 - \left[C_{GIT}(t) + C_{l,b}^{alv}(t) + C_{l,b}^{bb}(t) + C_{l,b}^{BB}(t)\right], \quad (10)$$

with C_{GIT}, $C_{l,b}^{alv}$, $C_{l,b}^{bb}$, and $C_{l,b}^{BB}$ representing the gastrointestinal tract compartment and lymph/blood compartments of the alveolar (alv), bronchiolar (bb), and bronchial (BB) region, respectively. As recognizable from the model and Eq. (10), $R(t)$ is highly dependent upon the fraction of deposited particles, f_s, being subject to slow clearance mechanisms. As outlined in earlier contributions [14,27], for spherical particles a linear relationship between f_s and the geometric particle diameter, d_g, can be formulated as follows:

$$f_s = 0.72 - 0.12d_g. \quad (11)$$

Concerning nonspherical particles, the application of d_g for the evaluation of f_s has to be regarded as unsuitable because it does not reflect the particle's real dimensions at all. In this case the equivalent projected area diameter, d_{ea}, seems to be more appropriate. For fibers with an aspect ratio >3 d_{ea} is defined by the formula

$$d_{ea} = \sin(\alpha)d_p + \cos(\alpha)\beta, \quad (12)$$

where α represents the angle of the fiber axis relative to the projection plane (Fig. 4), d_p the cylindrical diameter of the fibrous particle, and β the aspect ratio. Assuming a fiber with $d_p = 1$ μm and $\beta = 10$, which hits the projection plane with an angle $\alpha = 60°$, d_{ea} amounts to 5.85 μm, and f_s calculated according to Eq. (11) gives 0.018, i.e. 1.8% of the particles deposited are subject to slow clearance mechanisms.

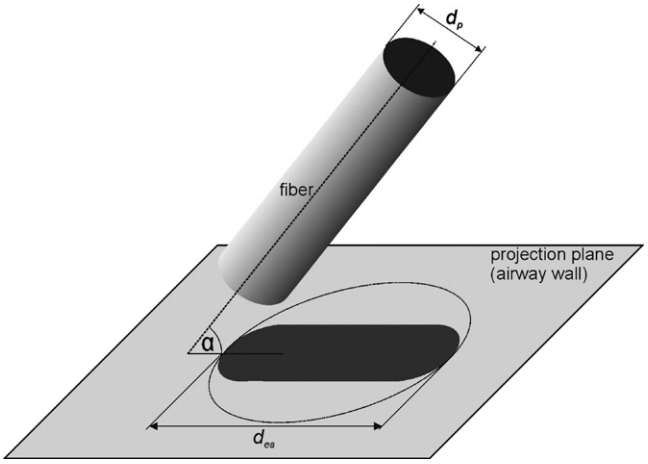

Fig. 4. Determination of the equivalent diameter d_{ea} of a fiber being randomly oriented with respect to the epithelial wall of a lung airway.

3. Results of theoretical modelling

3.1. Deposition of fibrous particles in the HRT

In order to demonstrate the effect of fiber length on the deposition of fibrous particles in the HRT, aspect ratio β of fibers used for the theoretical predictions was varied between 3 and 100. The cylindrical diameter of the fibers, d_p, ranged from 0.001 to 10 μm, covering a rather wide spectrum of inhalable particles. Respective aerodynamic diameters calculated with Eqs. (1)–(6) are summarized in Table 1. As can be noticed from the values listed in the table, for very small particles (0.001–0.01 μm) fiber length has only an insignificant influence on the aerodynamic diameter, with d_{ae} exceeding d_p by a factor of 1.3–1.4 for $\beta = 100$. The larger the model particles get, the higher is the difference between d_{ae} and d_p which finally amounts to 163.5% in the case of 10-μm fibers ($\beta = 100$).

Concerning total deposition of fibers, which by definition includes extrathoracic and thoracic deposition, the effect of fiber length is again nearly negligible for small particles, but highly remarkable for large particles (Fig. 5). Independent of the breathing conditions selected for the simulations, differences in total deposition between fibers with $\beta = 3$ and fibers with $\beta = 100$ are on the order of a few percent for fiber diameters ranging from 0.001 to 0.01 μm and become slightly increased for diameters ranging from >0.01 to 0.2 μm. Fibrous particles with diameters >0.2 μm exhibit most significant dependences of total deposition on fiber length, with discrepancies of the deposition curves for $\beta = 3$ and $\beta = 100$

Table 1
Aerodynamic diameters d_{ae} for fibers with different cylindrical diameters d_p and aspect ratios β.

	Aspect ratio β					
d_p	3	10	20	30	50	100
0.001	0.0011	0.0013	0.0013	0.0013	0.0013	0.0013
0.002	0.0022	0.0025	0.0026	0.0027	0.0027	0.0026
0.005	0.0054	0.0064	0.0066	0.0067	0.0068	0.0067
0.01	0.011	0.013	0.013	0.014	0.014	0.014
0.02	0.022	0.026	0.028	0.028	0.029	0.029
0.05	0.057	0.069	0.074	0.077	0.080	0.083
0.1	0.12	0.15	0.16	0.17	0.184	0.19
0.2	0.26	0.33	0.37	0.38	0.41	0.44
0.5	0.78	0.99	1.10	1.16	1.23	1.32
1.0	1.57	1.99	2.20	2.32	2.46	2.63
2.0	3.13	3.97	4.40	4.63	4.91	5.27
3.0	4.70	5.96	6.60	6.95	7.37	7.90
5.0	7.83	9.93	11.00	11.58	12.28	13.17
10.0	15.65	19.85	22.00	23.17	24.57	26.35

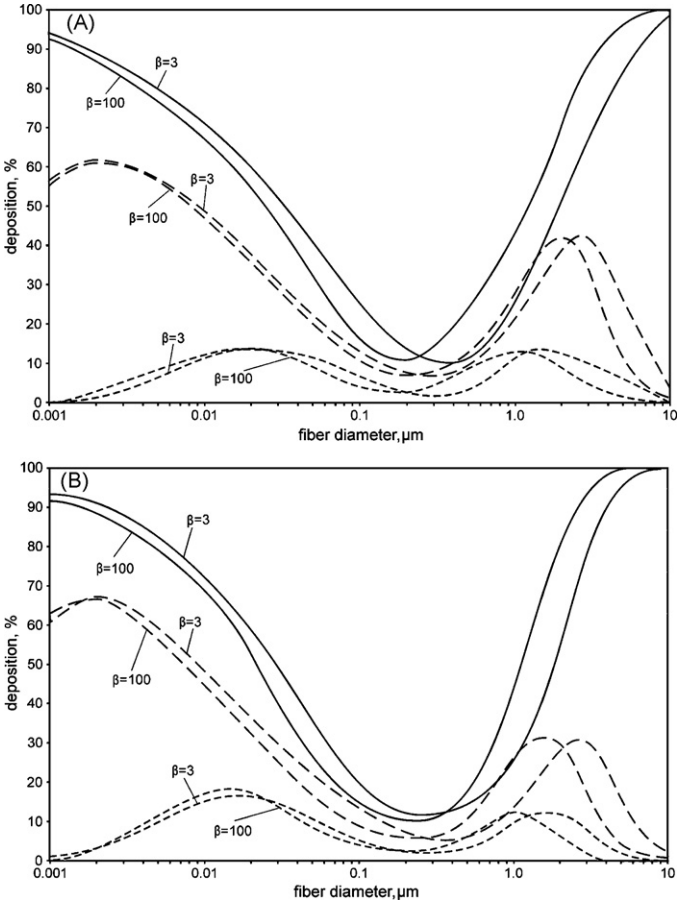

Fig. 5. Total (full lines), tubular (long-dashed lines), and alveolar (short-dashed lines) deposition for fiber diameters d_p ranging from 0.001 to 10 μm. To account for a possible influence of the fiber geometry (length), β was set to 3 and 100, respectively. (A) Sitting breathing conditions, (B) light-work breathing conditions [16].

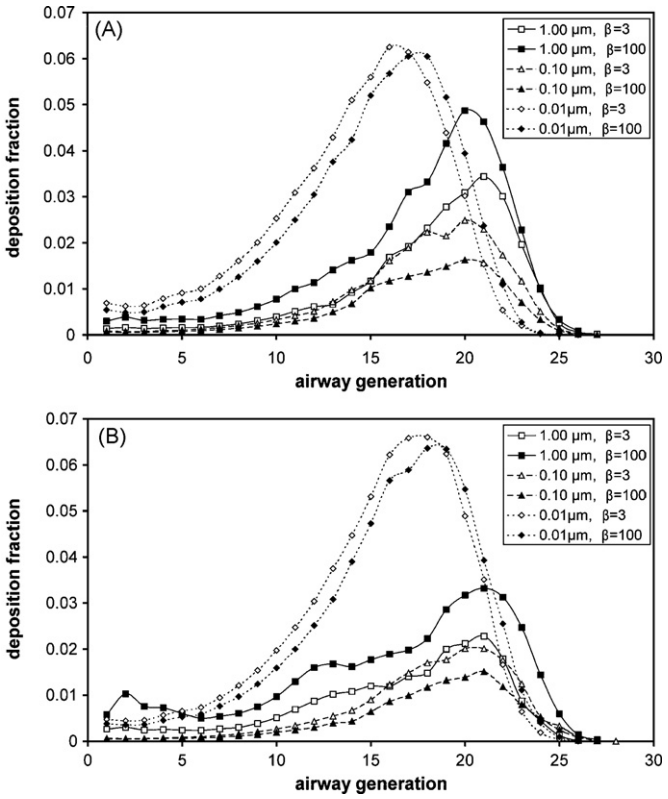

Fig. 6. Generation-by-generation deposition for 0.01, 0.1, and 1-μm particles with aspects ratios β of 3 and 100, respectively. To enable a comparison with the graphs of Fig. 5, deposition fractions are normalized to the total number of inhaled fibers. (A) Sitting breathing conditions, (B) light-work breathing conditions [16].

being on the order of 10–15%. Comparison of sitting breathing conditions (Fig. 5A) with light-work breathing conditions (Fig. 5 B) yields an enhancement of coarse particle deposition with increased inhalative flow, whereas the effect of fiber length on total deposition may be evaluated as rather independent of the given flow rate.

For the sake of completeness, also tubular (i.e. bronchial and bronchiolar) as well as alveolar deposition and its dependence on fiber diameter and length are illustrated in Fig. 5. Deposition differences caused by the length variability of inhaled fibers vary between 0% and 12% and are, again, dependent upon the diameter of the fibers. Tubular and alveolar deposition of fibers with d_p >0.2 μm is subject to a remarkable change with inhalative flow: first, maximum deposition is significantly declined with increasing flow rate, and second, half width of the deposition peaks is narrowed due to an increase of extrathoracic deposition for d_p ranging from 2 to 10 μm.

The effect of fiber dimensions and the inhalative flow on fiber deposition was additionally investigated by deposition-by-airway-generation graphs (Fig. 6). It has to be noted that the particle fraction entering the lungs was not normalized to 100%, so that a direct reference to Fig. 5 can be made. All deposition curves of Fig. 6 are characterized by a clear peak which is located between airway generation 15 and 21. The most proximal position of the deposition maximum is recognizable for fibers with $d_p = 0.01$ μm, while the other two fiber size classes used in this context ($d_p = 0.1$ μm and $d_p = 1.0$ μm) show respective maxima at more distal sites of the lung. Regarding the influence of β on bifurcation-specific particle deposition, both an enhancement and decline of deposition with increasing aspect ratio can be observed, and the position of the deposition peaks is subject to a slight shift either towards the trachea or towards the lung periphery (Fig. 6). Change of the inhalative flow rate mainly affects fibers with $d_p = 0.1$ and $d_p = 1.0$, whose deposition rates are significantly reduced, when switching from sitting to light-work breathing conditions. On the other hand, fibrous particles with $d_p = 0.01$ exhibit only slight modifications of their deposition patterns under the given breathing conditions.

3.2. Model validation – comparison of theoretical results with experimental data

Theoretical deposition results obtained from the model were compared with experimental data provided by Su and Cheng [1]. These authors measured fiber deposition in a realistic replica of the extrathoracic region and upper lung airways, thereby considering inspiratory flow rates of 15 and 43.5 l min^{-1}, which correspond to sitting breathing and light-working breathing conditions, respectively. For the experiments fibrous particles with a specific weight of 1.83 g cm^{-3}, a uniform diameter of 3.66 μm, and a length between 10 and 70 μm were used. In order to provide an appropriate comparison between experiment and model, morphometric data of the replica were used for theoretical computations. Additionally, only fiber deposition exclusively caused during inhalation was considered.

Concerning the first deposition scenario applying an inspiratory flow rate of 15 l min^{-1} and fibers with a length of 10–20 μm, good correspondence between experiment and model is obtained for airway generations 0–4 (Fig. 7A). Significant differences can be observed for the extrathoracic region, where model data exceed experimental results by a factor of 3. This effect causes a higher experimental fiber deposition in the trachea and the following

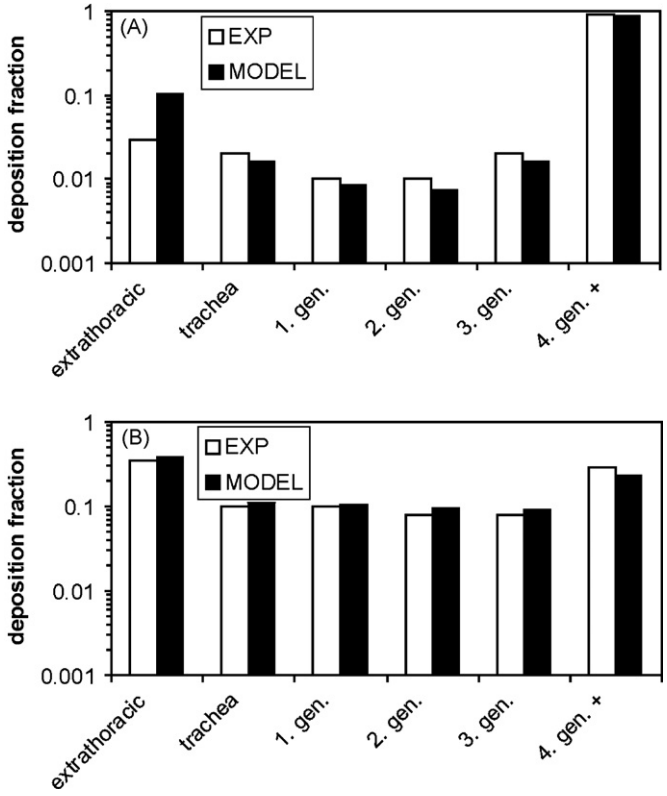

Fig. 7. Comparison of the experimental fiber deposition data outlined by Su and Cheng [6] with theoretical results which were obtained by using identical breathing conditions (Q: 15 and 43.5 l min^{-1}) and particle properties (d_p: 3.66 μm, fiber length: 10–70 μm, density: 1.83 g cm^{-3}).

airway bifurcations. Differences between theoretically and experimentally derived airway depositions are on the order of 10–15%.

In the second scenario, an inspiratory flow rate of 43.5 l min^{-1} and fibers with a length between 60 and 70 μm were selected. Now, discrepancies between model and experiment are almost negligible for the extrathoracic region, thereby being on the order of <10% (Fig. 7B). The same excellent correspondence is given for the airway generations 1–3, whereas for the following airway generations (gen. 4+) differences between model and experiment are subject to a slight increase. From these preliminary results it can be concluded that the agreement between model and experimental data is partly marked by high excellence, making the theoretical approach useful for further predictions of fiber deposition in future.

3.3. Clearance of fibers from the HRT

In the study presented here, clearance scenarios of fibers with different geometries ($\beta = 3$, $\beta = 100$) deposited in the HRT under sitting and light-work breathing conditions were simulated. Clearance efficiencies of respective particle classes were expressed by computing retention graphs based on Eq. (10) and 24-h retention values, which indicate the particulate mass that is still retained in the lungs 24 h after exposure to airborne particles. Concerning sitting breathing conditions, clearance of fibers with diameters ranging from 0.01 to 0.1 μm may be regarded as quite uniform with 24-h retention taking values between 0.802 and 0.837 (Table 2, Fig. 8A). While clearance of such small fibrous particles is rather independent of the aspect ratio, a contrary picture is given for particles with diameters ≥1 μm, where the related 24-h retention values range from 0.702 ($\beta = 100$) to 0.777 ($\beta = 3$). Both 24-h retention and clearance efficiency after 25 days depend on the fraction of particulate mass deposited in the small ciliated airways of the bronchiolar lung

Table 2
24-h retentions of fibrous particles (d_p: 0.01, 0.1, and 1 μm) with two different aspect ratios (3 and 100). To account for possible effects due to changes of the inhalative flow rate, sitting breathing and light-work breathing [16] are additionally compared.

	Sitting breathing		Light-work breathing	
d_p	$\beta = 3$	$\beta = 100$	$\beta = 3$	$\beta = 100$
0.01	0.802	0.813	0.834	0.849
0.10	0.837	0.814	0.829	0.828
1.00	0.777	0.702	0.769	0.706

region and in the alveoli (Fig. 5). Under the selected breathing conditions this fraction is smallest for 1-μm fibers with $\beta = 100$, which are chiefly subject to an extrathoracic and upper-bronchial deposition.

Under light-work breathing conditions fiber clearance changes insofar that most 24-h retention values become slightly increased with respect to those values obtained for sitting breathing conditions (Table 2). Despite a partly significant difference of the clearance behaviour during the first few days after particle inhalation, long-term clearance is quite uniform for all particles considered except for those with a diameter of 1 μm und $\beta = 100$, which are again cleared most effectively (Fig. 8B). However, after 25 days particulate mass retained in the HRT varies between 30% and 42% and thus deviates negligibly from the values computed for sitting breathing conditions. As already demonstrated in the earlier chapters of this work, change of the breathing conditions within the range considered here has only a slight effect on regional particle deposition, and since this parameter represents

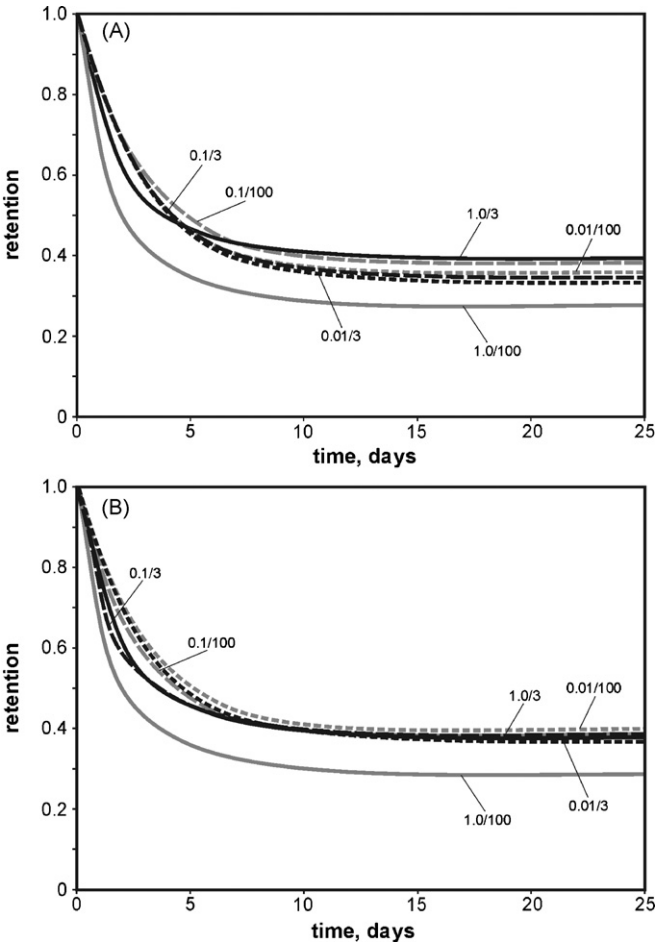

Fig. 8. Retention of fibrous particles with the same geometric characteristics as used for deposition calculations exhibited in Fig. 6. (A) Sitting breathing conditions, (B) light-work breathing conditions [16]. X/Y-values in the graphs indicate fiber diameter and aspect ratio, respectively.

a determinant of particle clearance, also the latter phenomenon is only insignificantly affected by changing the breathing frequency and tidal volume.

4. Discussion and conclusions

In the present contribution a mathematical model for the simulation of fiber deposition and clearance in the HRT was introduced. The necessity of this theoretical approach is mainly based on the circumstance that most deposition models published in the literature hitherto are restricted to a pre-determined sequence of (few) airway bifurcations [35–38], whereas simulation of fiber clearance has not found comparable scientific engagement [16]. However, the low number of fiber models for the HRT may be regarded as a result of the limitation of experiments to artificial, non-physiological casts and laboratory animals in the past decades [10]. In the meantime, replica of the upper HRT perfectly subsume natural shapes (oral cavity, larynx, etc.) and geometries, and measurements of deposited particle concentrations in such physiological casts have reached a remarkably increased level [1,5]. Regarding fiber clearance, animal data have become increasingly important for the human medical research, since it has been found that clearance mechanisms and velocities in the (monopodial) animal lungs are well comparable with those in human lungs.

Following earlier considerations with respect to fiber deposition, the aerodynamic diameter d_{ae} has been used as basic determinant for the description of fiber behaviour in the HRT. Although the geometry of a fiber, above all its axial dimension, does not find an appropriate expression by this complex parameter, the aerodynamic diameter concept has found a rather wide acceptance in the respective scientific field meanwhile [1,5,9,13], and alternative concepts with similar reliability have not been introduced so far. Deposition mechanisms such as interception and sedimentation, where fiber length may play an essential role, have been subject to mathematical corrections derived from specific numerical approaches [35–38]. As illustrated in Table 1, d_{ae} is rather insensitive to the aspect ratio β in the case of ultrafine particles (<0.1 μm), while β has an increased importance for the remaining particle classes (≥0.1 μm). This phenomenon is due to the fact that the influence of the equivalent volume diameter d_{ev} upon d_{ae} is largely neutralized by the ratio of the Cunningham slip correction factors $C_C(d_{ev})/C_C(d_{ae})$ of Eq. (1). The slip correction factors reach higher values for ultrafine particles and approximate to 1 with increasing particle diameter [13], so that for particles with a diameter greater than 0.1 μm the effect of d_{ev} on d_{ae} gets back its significance.

As indicated by the graphs of Fig. 5, total as well as tubular and alveolar deposition depend on β in the way that deposition curves of fibers with $\beta = 100$ are slightly shifted towards smaller particle diameters. Detailed analysis of the graphs results in the conclusion that fibers with a diameter <0.2 μm exhibit a negative correlation with the aspect ratio, while for fibers with a diameter ≥0.2 μm the respective deposition parameters and β are characterized by a positive correlation. From these results the following essential conclusions can be drawn: (1) For ultrafine particles, increasing fiber length causes a reduction of particle deposition by Brownian diffusion, finally resulting in a slight enhancement of the exhaled particle fraction. (2) For larger particles (≥0.2 μm), increase of the aspect ratio significantly affects particle deposition by impaction, interception, and sedimentation. Differences of deposition between short and long fibers are more pronounced within this size category (Fig. 5A).

A change from sitting breathing to light-work breathing has only insignificant effects on total fiber deposition (Fig. 5B), with increasing β resulting in the same phenomenon as already noted above. Contrary to the sitting breathing scenario, total deposition curves derived from the theoretical model are characterized by broader minima, indicating a wider particle size range that behaves rather insensitive with respect to the main deposition forces [16,25]. Concerning tubular and alveolar fiber deposition, modification of the breathing conditions has the following consequences: (1) the alveolar deposition fraction is slightly enhanced for ultrafine particles, but remains nearly constant for particles ≥0.2 μm. (2) Tubular deposition is slightly increased for ultrafines, but strongly reduced (up to 30% with respect to sitting breathing) for larger particles, whereby most of this reduction takes place for the benefit of extrathoracic deposition. Summing up, it can be concluded that an enhancement of the inhalative flow rate causes increased lung deposition of ultrafine fibers and enhanced extrathoracic deposition of larger fibers, thereby exhibiting similar effects as in the case of spherical particles [16,25].

Regarding the generation-by-generation deposition of fibers most of the characteristics outlined for total deposition can be found again in the respective graphs (e.g. dependence of deposition on β). Highest deposition per airway generation could be obtained for fibers with a diameter of 0.01 μm, while lowest deposition was determined for fibers with a diameter of 0.1 μm (Fig. 6), because the latter size class plots close to the minimum of the total deposition curves illustrated in Fig. 5. Deposition maxima are positioned between airway generation 17 and 21. Changes of the breathing conditions mainly affect the fibrous particles with a diameter of 1.0 μm, being subject to enhanced inertial impaction with increasing inhalative flow rate and thus showing similar intrapulmonary transport characteristics as 1-μm spheres [16]. From the local deposition graphs it can be concluded that (1) ultrafine fibers (d_p <0.1 μm) independent of their length and the breathing conditions preferentially deposit in intermediately to terminally situated lung airways, thereby representing a remarkable health hazard, and (2) local deposition of larger fibers is more effectively influenced by β and the breathing parameters, with shortening of the breathing cycle leading to an enhancement of particle filtering in the proximal airways [16].

Independent of fiber geometry and breathing conditions, clearance of fibrous particles from the HRT is characterized by a fast stage with a half-time of less than 24 h and an efficiency ranging from 30% to 50%. This fast clearance is typically followed by an intermediate stage with a half-time of about 5 days and an efficiency of 10–20%. The last stage is a long-term clearance with half-times being on the order of several months and reduction of the retained particle mass being much less than 1% per day (Fig. 8). Subdivision of clearance into a fast, intermediate, and slow phase has been frequently described for spherical particles in the past [14,26,27], whereby the fast stage exclusively corresponds with mucociliary clearance, the intermediate stage with slow bronchial clearance, and the slow stage with alveolar clearance. Lung clearance and its percentile subdivision into the three phases is to a high extent controlled by the deposition pattern of a certain fiber class, so that β and the inhalative flow rate may be characterized by either a mutual decrease or a reciprocal amplification [1,5,16]. A main drawback of the currently used clearance model concerns the fact that many clearance rates highly depend on the shape and composition of the deposited particles. For instance, uptake of long fibers by macrophages needs more time than that of spheres, and respective clearance is significantly retarded. Further, fibers undergo splitting and breakage during their residence on the lung airway surface, so that the physicochemical properties of these particles become highly essential for any clearance computations. These points will be considered in future model refinements.

From the preliminary modelling results presented in this contribution, it may be concluded that the theoretical approach might provide valuable deposition and clearance data for fibrous particles in the future, provided that a continuous model refinement on the basis of experimental results will be enabled.

References

[1] W.C. Su, Y.S. Cheng, Deposition of fiber in a human airway replica, J. Aerosol Sci. 37 (2006) 1429–1441.
[2] T.W. Hesterberg, G.A. Hart, Synthetic vitreous fibers: a review of toxicology research and its impact on hazard classification, Crit. Rev. Toxicol. 31 (2001) 1–53.
[3] O. Kamstrup, A. Ellehauge, C.G. Collier, J.M.G. Davies, Carcinogenicity studies after intraperitoneal injection of two types of stone wool fibres in rats, Ann. Occup. Hyg. 46 (2002) 135–142.
[4] NIOSH, Asbestos and other fibers by PCM, NIOSH manual of analytical method.
[5] W.C. Su, Y.S. Cheng, Deposition of fiber in the human nasal airway, Aerosol Sci. Technol. 39 (2005) 888–901.
[6] T. Myojo, M. Takaya, Estimation of fibrous aerosol deposition in upper bronchi based on experimental data with model bifurcation, Ind. Health 39 (2001) 141–149.
[7] T. Myojo, Deposition of fibrous aerosol in model bifurcating tubes, J. Aerosol Sci. 18 (1987) 337–347.
[8] R.G. Sussmann, B.S. Cohen, M. Lippmann, Asbestos fiber deposition in human tracheobronchial cast. I. Experimental, Inh. Toxicol. 3 (1991) 145–160.
[9] W. Stöber, H. Flachsbart, D. Hochrainer, The aerodynamic diameter of latex aggregates and asbestos fibres, Staub-Reinhalt Luft 30 (1970) 1–12.
[10] M. Lippmann, Effects of fiber characteristics on lung deposition, retention, and disease, Environ. Health Perspect. 88 (1990) 311–317.
[11] A. Morgan, A. Holmes, The deposition of MMMF in the respiratory tract of the rat, their subsequent clearance, solubility in vivo and protein coating, in: WHO, Biological effects of man-made mineral fibers, vol. 2, World Health Organization, Copenhagen, 1984, pp. 1–17.
[12] A. Morgan, A. Black, N. Evans, A. Holmes, J.N. Pritchard, Deposition of sized glass fibers in the respiratory tract of the rat, Ann. Occup. Hyg. 23 (1980) 353–366.
[13] Y.T. Dai, C.P. Yu, Alveolar deposition of fibers in rodents and humans, J. Aerosol. Med. 11 (1998) 247–258.
[14] R. Sturm, W. Hofmann, G. Scheuch, K. Sommerer, M. Svartengren, P. Camner, Particle clearance in human bronchial airways: comparison of stochastic model predictions with experimental data, Ann. Occup. Hyg. 46 (Suppl. 1) (2002) 329–333.
[15] W. Kreyling, G. Scheuch, Clearance of particles deposited in the lungs, in: P. Gehr, J. Heyder (Eds.), Particle-Lung Interactions, Marcel Dekker, Inc., New York, 2000, pp. 323–376.
[16] International Commission on Radiological Protection (ICRP), Human respiratory tract model for radiological protection, Publication 66, Ann. ICRP, Pergamon Press, Oxford, 1994.
[17] A. Morgan, A. Holmes, W. Davison, Clearance of sized glass fibers from the rat lung and their solubility in vivo, Ann. Occup. Hyg. 25 (1982) 317–331.
[18] V. Timbrell, Deposition and retention of fibers in human lung, Ann. Occup. Hyg. 26 (1982) 347–369.
[19] K. Horsfiled, G. Dart, D.E. Olson, G.F. Filley, G. Cumming, Models of the human bronchial tree, J. Appl. Physiol. 31 (1971) 207–217.
[20] D.B. Taulbee, C.P. Yu, A theory of aerosol deposition in the human respiratory tract, J. Appl. Physiol. 38 (1975) 77–85.
[21] T.T. Soong, P. Nicolaides, C.P. Yu, S.C. Soong, A statistical description of the human tracheobronchial tree geometry, Resp. Physiol. 37 (1979) 161–172.
[22] C.P. Yu, P. Nicolaides, T.T. Soong, Effect of random airway sizes on aerosol deposition, Am. Ind. Hyg. Assoc. J. 40 (1979) 999–1005.
[23] W. Hofmann, F. Daschil, Biological variability influencing lung dosimetry for inhaled ^{222}Rn and ^{220}Rn, Health Phys. 50 (1986) 345–367.
[24] H. Yeh, G.M. Schum, Models of Human lung airways and their application to inhaled particle deposition, Bull. Math. Biol. 42 (1980) 461–480.
[25] L. Koblinger, W. Hofmann, Monte Carlo modeling of aerosol deposition in human lungs. Part I. Simulation of particle transport in a stochastic lung structure, J. Aerosol Sci. 21 (1990) 661–674.
[26] R. Sturm, W. Hofmann, A multicompartment model for bronchial clearance of insoluble particles in the human lung, Rad. Prot. Dosim. 118 (2006) 384–394.
[27] W. Hofmann, R. Sturm, Stochastic model of particle clearance in human bronchial airways, J. Aerosol Med. 17 (2004) 73–89.
[28] C.P. Yu, J.P. Hu, B.M. Yen, D.M. Spektor, M. Lippmann, Models for mucociliary particle clearance in lung airways, in: S.D. Lee, T. Schneider, L.D. Grant, P.J. Verkerk (Eds.), Aerosols: Research, Risk Assessment and Control Strategies, Lewis, Chelsea, MI, 1986, pp. 569–578.
[29] R.G. Cuddihy, H.C. Yeh, Respiratory tract clearance of particles and substances dissociated from particles, in: U. Mohr (Ed.), Inhalation Toxicology: The Design and Interpretation of Inhalation Studies and their use in Risk Assessment, Springer, Berlin, 1988, pp. 169–193.
[30] W. Stöber, Dynamic shape factors of nonspherical aerosol particles, in: T.T. Mercer (Ed.), Assessment of Airborne Particles, Charles C Thomas Publisher, Springfield, 1972, pp. 249–289.
[31] J. Happel, H. Brenner, Low Reynolds number hydrodynamics, Noordhoff, Leyden (1973).
[32] O.G. Raabe, H.C. Yeh, G.M. Schum, R.F. Phalen, Tracheobronchial geometry: human, dog, rat, hamster—a compilation of selected data from the project respiratory tract deposition models, Report LF-53, Lovelace Foundation, Albuquerque, New Mexico, 1976.
[33] B. Haefeli-Bleuer, E.R. Weibel, Morphometry of the human pulmonary acinus, Anat. Rec. 220 (1988) 401–414.
[34] L. Koblinger, W. Hofmann, Analysis of human lung morphometric data for stochastic aerosol deposition calculations, Phys. Med. Biol. 30 (1985) 541–556.
[35] I. Balásházy, W. Hofmann, Particle deposition in airway bifurcations: I. Inspiratory flow, J. Aerosol Sci. 24 (1993) 745–772.
[36] I. Balásházy, W. Hofmann, Particle deposition in airway bifurcations: II. Expiratory flow, J. Aerosol Sci. 24 (1993) 773–786.
[37] F.S. Cai, C.P. Yu, Inertial and interceptional deposition of spherical particles and fibers in a bifurcating airway, J. Aerosol Sci. 19 (1988) 679–688.
[38] Y.K. Chen, C.P. Yu, Sedimentation of fibers from laminar flows in a horizontal circular duct, Aerosol Sci. Technol. 14 (1991) 343–347.
[39] Z. Wang, P.K. Hopke, G. Ahmadi, Y.S. Cheng, P.A. Baron, Fibrous particle deposition in human nasal passage: the influence of particle length, flow rate, and geometry of nasal airway, J. Aerosol Sci. 39 (2008) 1040–1054.
[40] B. Dahneke, Slip correction factors for nonspherical bodies—II free molecule flow, J. Aerosol Sci. 4 (1973) 147–161.
[41] B. Asgharian, S. Anjilvel, Movement and deposition of fibers in an airway with steady viscous flow, Aerosol Sci. Technol. 22 (1995) 261–270.
[42] M. Shams, G. Ahmadi, H. Rahimzadeh, Transport and deposition of flexible fibers in turbulent duct flows, J. Aerosol Sci. 32 (2001) 525–547.
[43] I. Balásházy, T.B. Martonen, W. Hofmann, Fiber deposition in airway bifurcations, J. Aerosol Med. 3 (1990) 243–260.